Complex Wave and Phase Retrieval from A Single Off-Axis Interferogram: supplemental document

This document provides supplementary information to "Complex Wave and Phase Retrieval from A Single Off-Axis Interferogram: supplemental document". The examples of simulation about complex wave retrieval and phase restoration under high noisy conditions are provided. Then, we describe experimental settings of real experiments. And more results of real experimental data about phase retrieval with respect to interfeorgram with overlap, large amplitude ratio of object to reference waves are given.

1. EXTRA SIMULATION RESULTS

First, we investigate the complex wave reconstruction quality under high noisy conditions. In the simulation, we use the same synthetic 'Spoke' phase image (512×512 pixels, large phase range [-0.2, 2.7] radians) as Fig. 8. And for comparison, Baek's algorithm [1], the classical FT approach and a recent total variation-based compressing sensing (CS) method [2] are chosen. The reference wave intensity is provided for Baek's approach. The definitions of amplitude ratio between object to reference waves (O/R), numerical overlap (NO), radius of circular support (ρ), and reference wave frequencies (k_x, k_y) can be referred to the primary paper.

Figure S1 shows the real-part images of the reconstructed complex-valued object wave from the simulated noisy interferogram with Additive white Gaussian noise (AWGN) in PSNR of 10 dB. The regularization parameter in the CS method is set to 40 under the high noisy case (suggested in [2]). Clearly, our complex wave retrieval (CWR) achieves a much better quality of reconstruction than other approaches. Obviously, fringe-like artifacts can be seen in Baek's and FT's algorithms, which likely come from unsuccessful suppression of the zeroth order. The FT method doesn't allow the frequency overlap between zeroth order and twin images of the interferogram, thus it exhibits poor quality. The CS method could reduce the noise and preserve the edges but at the expense of a significantly high computational time. In this example, it has less good resolution near the fast varying center area compared to our result (see zoomed box), which may depend on the selected regularization parameter. Furthermore, a high-resolution experiment (see Fig. S2) is also provided under larger object bandwidth and numerical overlap, higher amplitude ratio but less noise on the interferogram, in which high-frequency components correspond to the rapid variations around the image center.
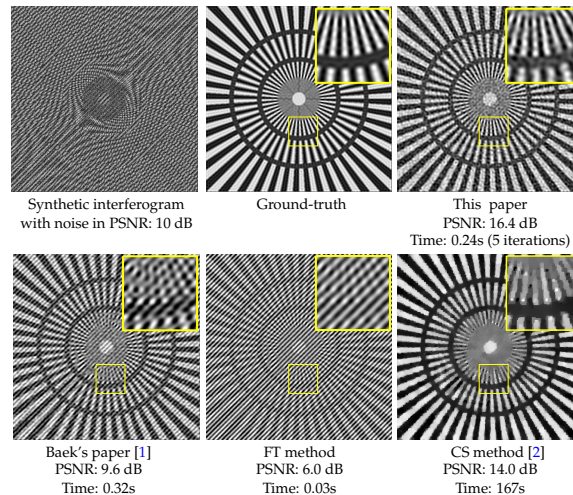

| Synthetic interferogram with noise in PSNR: 10 dB | Ground-truth | This paper
PSNR: 16.4 dB
Time: 0.24s (5 iterations) |
| Baek's paper [1]
PSNR: 9.6 dB
Time: 0.32s | FT method
PSNR: 6.0 dB
Time: 0.03s | CS method [2]
PSNR: 14.0 dB
Time: 167s |

Fig. S1. Higher quality of reconstruction by our complex wave retrieval algorithm than others under simulated noisy interferogram (O/R = 0.7, NO = 1.3, $\rho = \sqrt{2\pi}/3$ and $k_x = k_y$). The reconstructed images (real-part only) images are shown in the same scale for comparison.
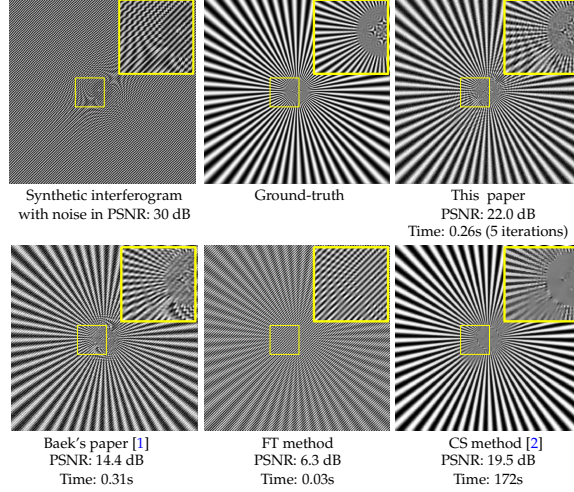
Fig. S2. A higher resolution of reconstruction by our complex wave retrieval algorithm than other methods under less noisy interferogram but higher $O/R = 1.1$, $NO = 2$, $\rho = \sqrt{2\pi}/1.1$ ($k_x = k_y$). The reconstructed images (real-part only) are shown in the same scale.

Then, we carry out simulation to verify the robustness of proposed restoration algorithm under noisy cases. Here, the conventional restoration is chosen for comparison, consisting of phase unwrapping and polynomial fit two steps. Two open-source phase unwrapping algorithms of PUMA [1] [3] and TIE [2] [4] are used in the conventional restoration (not in ours).

In the simulation, we use the same USAF phase image (512×512 pixels with a large range of values $\in [-0.31, 2.54]$ radians) as that in Fig. 9. It is distorted by a 2D Chebyshev polynomial of degree 4, further corrupted by AWGN. We ensured the range of the ground-truth phase with noise is within [-π, π] radians. In the following Fig. S3, the ground-truth phase image is with noise in PSNR of 10 dB. By comparing the experimental results of restoration in Fig. S3, our restoration achieves similar quality as other unwrap-and-fit approaches. We have tried different noise levels, all methods are able to remove the distortion correctly from the noisy wrapped phase. But our algorithm executes faster than others, especially than the unwrap [3]-and-fit approach.
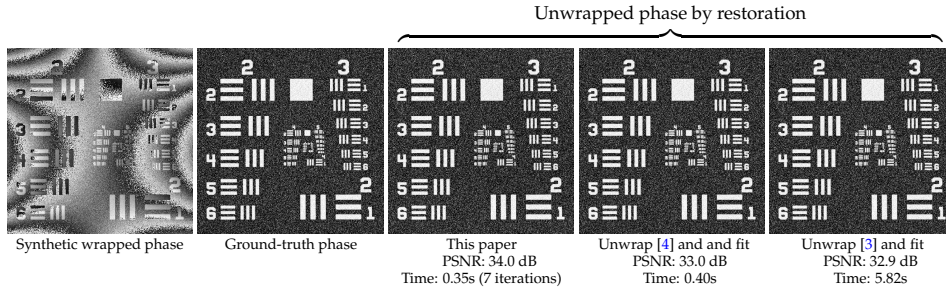

Fig. S3. Almost the same quality (PSNR>30 dB) of restoration by all methods from the simulated noisy wrapped phase (512×512 pixels). Here, a polynomial of degree 4 is used to fit the distortion.

2. EXTRA REAL EXPERIMENTAL RESULTS

A. Experimental Setting

For the real experiments, we utilized a Mach-Zehnder interferometer with a laser pointer (Model No. CPS532, Thorlabs) with a wavelength of 532 nm. In order to test the maximum allowed bandwidth for the object wave, we choose a microscope objective (MO) lens with a large numerical

---

[1] http://www.lx.it.pt/~bioucas/code.htm
[2] https://ww2.mathworks.cn/matlabcentral/fileexchange/68493-robust-2d-phase-unwrapping-algorithm

aperture (NA) based on the microscope cut-off frequency defined in Eq. (13) in Ref. [5]. The relevant essential optical hardwares used in each experiment are:

1. (in Fig. 10, Fig. 11, Fig. S4) a MO (20X/0.8, Plan-Apochromat, Zeiss), and a monochrome camera (Model No. ORX-10GS-51S5M-C, Sony Imax250) with a 3.45 μm pixel size.
2. (in Fig. 12 and Fig. S5) a MO (20X/0.8, Plan-Apochromat, Zeiss), and a monochrome camera (Model No. BFS-U3-13Y3M-C, FLIR Systems) with a 4.8 μm pixel size.
3. (in Table S1 when $\rho = 0.6$) a MO (40X/0.65 NA, Plan-N, Olympus) and a monochrome camera (Model No. ORX-10GS-51S5M-C, Sony Imax250) with a 3.45 μm pixel size.

The focal length of the MO tube lens is 175 mm in all experiments. During the experiments, various numerical overlaps of interferogram are achieved by changing the slanted angle between the reference and object waves. And different amplitude ratios between the object to reference waves are realized by tuning the thin-film linear polarizers (Model No. LPVISE100-A, Thorlabs) placed in the two light paths of the interferometer.

B. Phase Restoration

First, we apply the proposed restoration algorithm in this paper to the raw wrapped phase in Fig. 10 obtained by each complex wave retrieval method. The results are shown in the following Fig. S4. Here, the conventional restoration of TIE unwrap [4] and fit are carried out as well. As the same as that in Fig. 10, a polynomial of degree 4 (first 10 polynomials) is used to fit the distortion. Based on the relation between phase ϕ_o introduced by object and height values h_o in quantitative phase imaging, namely $\phi_o = \frac{2\pi}{\lambda} \Delta n h_o$ [6–8], we also provide the height profiles in the insets of Fig. S4 along the red dashed line. $\Delta n = 0.52$ is refractive index differences between the object and the surrounding medium. The standard phase deviation in the object-free area (Outliers e.g. over-saturated values are excluded) is also calculated.
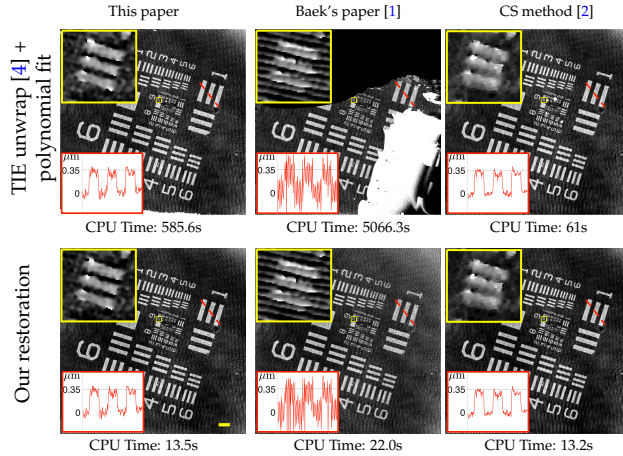

Fig. S4. Not only the computational efficiency but also the much better quality of restored phase (especially for Baek's result) by proposed restoration in this paper are greatly improved compared to the results via conventional restoration in Fig. 10. Scale bar indicates 20 μm.

By comparing the different restored phase images in each column in Fig. S4 and in Fig. 10 (bottom), the proposed restoration is more robust to the high-frequency fringe corruption and can effectively avoid the unwrapping errors induced by rapid phase variations. Meanwhile, the computational efficiency is greatly improved by the proposed restoration.

C. Imaging of Biomedical Cells

Then an additional example of phase restoration is provided when the phase unwrapping is needed after our restoration. In the experiment, the interferogram (1024×1024 pixels) of L929 cells is acquired. As shown in Fig. S5, the wrapped phase of the cells is reconstructed from the interferogram with a full overlap (NO = 1.76) by our CWR. A first 8 2D polynomial is sufficient to estimate well the global phase distortion of the complex-valued object wave. Because the restored phase (middle image in Fig. S5) introduced by the cell is larger than 2π radian, we further applied unwrapping algorithm to it. Almost the same quality of retrieved phase is obtained for

the both methods. However, by comparing computational time with the conventional restoration of unwrap [3] and fit, our algorithm combined with unwrap [3] is almost 2.8 times faster than that by unwrap [3]-and-fit method.
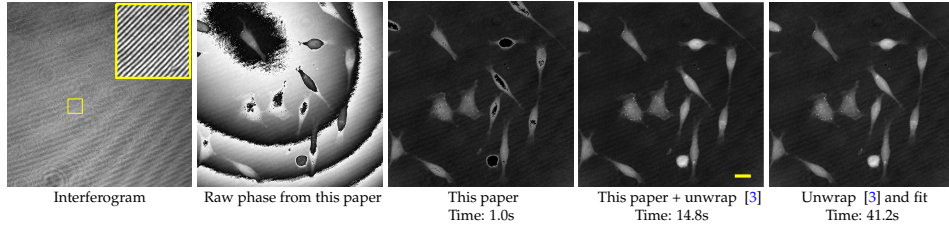

| Interferogram | Raw phase from this paper | This paper Time: 1.0s | This paper + unwrap [3] Time: 14.8s | Unwrap [3] and fit Time: 41.2s |

Fig. S5. Phase unwrapping is needed after our phase restoration since the cell-induced phase variations are beyond 2π. Our restoration combined with the phase unwrapping achieves the similar quality as the conventional restoration, but with a much faster speed. The standard phase deviations in the same object-free region are at the same level of 0.20 radians (≈ 17 nm height value) for both methods. Scale bar indicates 20 μm.

D. Influence of Amplitude Ratio

Finally, we investigate the object wave reconstruction under large amplitude ratios between the object to reference waves by the comparing the standard phase deviations in the object-free region (Outliers are excluded) . In the experiments, we capture interferograms with and without frequency overlaps for the same USAF phase target as Fig. S4, then apply the complex wave retrieval and phase restoration to obtain the quantitative phase.

As shown in Table S1, we calculate the standard deviation of phase retrieved from interferograms under large amplitude ratios and large (top row) or small (bottom row) numerical overlaps. The results show the CS method combined with conventional restoration (unwrap [3] and fit) achieves the smallest phase noise. Our algorithms obtain slightly larger standard phase deviations which are significantly smaller than that via Baek's CWR combined with conventional restoration especially under larger NO and ρ. Overall, the proposed CWR method still works well under high amplitude ratio conditions. It would be more promising if combined with some denoised work when there is large noise.

Table S1. Comparison of standard phase deviation in object-free region

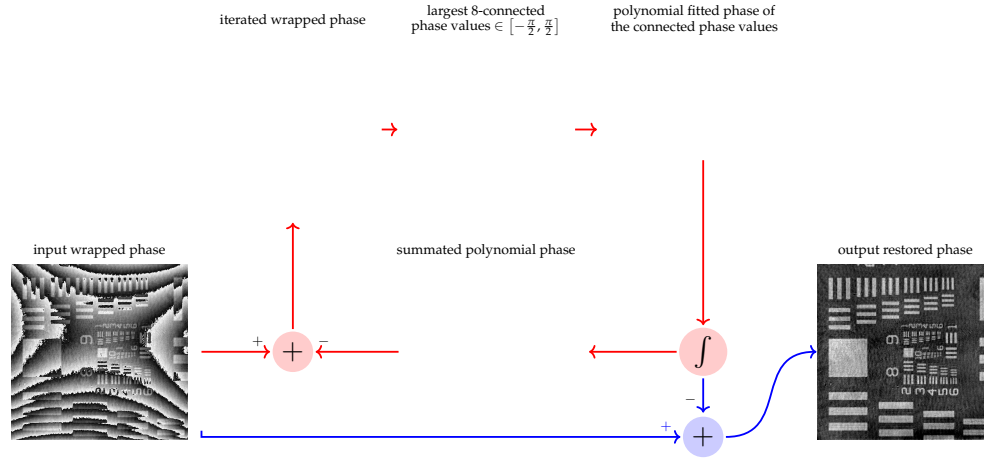| Interferogram condition	Our CWR + our restoration	Baek CWR [1] + unwrap [3] and fit	CS CWR [2] + unwrap [3] and fit
O/R = 1.34; NO = 0.8; $\rho = \pi/2$	0.27 radians (≈ 44 nm height value)	0.38 radians (≈ 62 nm height value)	0.21 radians (≈ 34 nm height value)
O/R = 1.61; NO = -0.1; $\rho = 0.6$	0.18 radians (≈ 29 nm height value)	0.21 radians (≈ 34 nm height value)	0.16 radians (≈ 26 nm height value)

3. FLOW CHART ANIMATION

Fig. S6. The animation of the phase restoration algorithm. Red/blue: iterated/non-iterated parts. The "$\int$" block denotes a summation over all previous iterates. The connected pixels are denoted by the red-colored region.

REFERENCES

1. Y. Baek, K. Lee, S. Shin, and Y. Park, "Kramers–Kronig holographic imaging for high-space-bandwidth product," Optica **6**, 45–51 (2019).
2. S. Yoshida, "Compressed off-axis digital holography," J. Opt. **22**, 095703 (2020).
3. J. M. Bioucas-Dias and G. Valadao, "Phase Unwrapping via Graph Cuts," IEEE Transactions on Image Processing **16**, 698–709 (2007).
4. Z. Zhao, H. Zhang, Z. Xiao, H. Du, Y. Zhuang, C. Fan, and H. Zhao, "Robust 2D phase unwrapping algorithm based on the transport of intensity equation," Meas. Sci. Technol. **30**, 015201 (2018).
5. N. Pavillon, C. S. Seelamantula, J. Kühn, M. Unser, and C. Depeursinge, "Suppression of the zero-order term in off-axis digital holography through nonlinear filtering," Appl. Opt. **48**, H186–H195 (2009).
6. B. Bhaduri, C. Edwards, H. Pham, R. Zhou, T. H. Nguyen, L. L. Goddard, and G. Popescu, "Diffraction phase microscopy: principles and applications in materials and life sciences," Adv. Opt. Photonics **6**, 57–119 (2014).
7. M. Niu, G. Luo, X. Shu, F. Qu, S. Zhou, Y.-P. Ho, N. Zhao, and R. Zhou, "Portable quantitative phase microscope for material metrology and biological imaging," Photonics Res. **8**, 1253–1259 (2020).
8. Y. Park, C. Depeursinge, and G. Popescu, "Quantitative phase imaging in biomedicine," Nat. Photonics **12**, 578–589 (2018).